Symmetrical capacitive deionization battery enabling dual capture of fluoride and copper ions

Qisheng Huang[1, a], Meiying Du[1, a], Lei Huang[a, b, *], Jia Yan[a, c], Xingtong Liang[a], Shaojian Xie[a], Hongguo Zhang[a, c, *], Meng Li[a], Shaocheng Chen[a], Hongbo Zeng[b, *]

a School of Environmental Science and Engineering, Guangzhou University, Guangzhou 510006, China

b Department of Chemical and Materials Engineering, University of Alberta, Edmonton, Alberta T6G 1H9, Canada

c Guangzhou University-Linköping University Research Center on Urban Sustainable Development, Guangzhou University, Guangzhou 510006, China

* Corresponding author at School of Environmental Science and Engineering, Guangzhou University, Guangzhou Higher Education Mega Center, Guangzhou 510006, China. E-mail address: huanglei@gzhu.edu.cn, hgzhang@gzhu.edu.cn, hongbo.zeng@ualberta.ca.

[1] These authors have equally contributed to the work.

Experimental Section

Chemicals and materials

Lithium iron phosphate is purchased from a battery recycling plant. Activated carbon (AC) and N-methylpyrrolidone (NMP, 99.0%) are purchased from Shanghai McLean Biochemical Co., Ltd., and acetylene black (AB) is purchased from Guangdong Kande New Energy Technology Co., Ltd. Polyvinylidene fluoride (PVDF) is purchased from Arkema (France). Sodium fluoride (NaF), hydrochloric acid (HCl), sodium hydroxide (NaOH), and glacial acetic acid (CH_3COOH) are purchased from Shanghai Aladdin Bio-Chemical Technology Co., Ltd. Sodium chloride (NaCl), sodium nitrate ($NaNO_3$), sodium sulphate (Na_2SO_4), sodium bromide (NaBr), and sodium phosphate (Na_3PO_4) are all supplied by Guangzhou Chemical Reagent Factory. The experimental water used is ultra-pure water with a conductivity of 18.25 M Ω-cm.

Materials characterization

The morphology of the materials is examined using scanning electron microscopy (SEM) and transmission electron microscopy (TEM). The composition and crystal structure of the materials are analyzed using X-ray diffraction (XRD). The specific surface area of the material, as well as the pore size distribution, is measured by a specific surface area and pore analyzer (BET). The functional groups in the materials are characterized by Fourier infrared spectroscopy (FT-IR). The surface elements and elemental composition of the materials are determined by X-ray photoelectron spectroscopy (XPS).

Preparation and experimentation of CDI

All electrodes used for CDI testing are prepared by uniformly coating electrode paste onto 4 × 4 cm^{-2} titanium plates. The paste is prepared by mixing active material ($LiFePO_4$), acetylene black (AB), and PVDF in an 8:1:1 mass ratio in N-methylpyrrolidone. The electrodes are then dried in a vacuum at 60°C before use. For the counter electrode, activated carbon (AC) is used as a substitute for the active

material, with all other conditions identical to those of the working electrode.

The CDI experiment is conducted in a custom-made CDI device. The electrodes are positioned parallel to each other on either side of the device, with a silicone sheet as a separator in between.

Fluoride Ion Removal Experiment

Set the peristaltic pump to pump 50 mL of a solution of a certain concentration of NaF ($CuF_2 \cdot H_2O$) into the CDI device at a certain flow rate. After the device has been running for 6 hours, extract the solution as the experimental solution. Mix the experimental solution with buffer solution (TISAB) in a 4:1 ratio to form the test solution. Use a fluoride ion electrode (CHN090) to determine the concentration Ce, and calculate the adsorption capacity Q using the formula:

$$SAC = \frac{(C_0 - C_t) \times V}{m}$$

$$SAR = \frac{SAC}{t}$$

C_0 and C_t are the initial concentration and the concentration after capacitive deionization of the solution, respectively. V is the volume of the solution, which is 0.05 L unless otherwise specified. m is the mass of the active material.

Preparation of buffer solution (TISAB)

Take 5 g of $Na_3C_6H_5O_7 \cdot 2H_2O$ and 29 g of NaCl and dissolve them in 400 mL of ultrapure water. Then add 28.5 mL of glacial acetic acid. Stir until the solute is completely dissolved, then use 0.01 mol L^{-1} HCl to control the pH of the mixed solution within the range of 5.0-5.5. Dilute the mixture to 500 mL and set aside.

Testing Method for Fluoride

The fluoride ion content in the solution was determined using a composite fluoride ion test electrode. This method established a calibration standard curve by calibrating the electrode with 1 ppm, 10 ppm, and 100 ppm fluoride ion standard solutions. Subsequently, 40 ml of desalinated solution was placed in a white plastic bottle, to

which 10 ml of TISAB was added and thoroughly mixed. The calibrated fluoride ion electrode was then inserted into the solution. After stabilizing for 10 seconds, the fluoride ion concentration was recorded.

Testing Method for Copper

To determine the concentration of Cu^{2+} following deionization, a 0.5 mL sample was taken from the collection beaker at the preset operating time. Copper reagent, ammonia solution and the test sample were mixed in a 25 mL colorimetric tube at a ratio of 15:1:1. The mixture was shaken thoroughly and allowed to stand for five minutes. Place the settled test solution in a UV-visible spectrophotometer (UV-1100, MAPADA) and measure at a wavelength of 452 nm.

Electrochemical measurements

All electrodes used for electrochemical measurements are pre-fabricated by applying electrode slurry to graphite paper sheets. This slurry is prepared by mixing active material, acetylene black (AB), and polyvinylidene fluoride (PVDF). The active material, acetylene black (AB), and PVDF are mixed in an 8:1:1 mass ratio in N-methylpyrrolidone (NMP). The electrodes are then dried overnight at 60 °C before use. The electrochemical properties of $LiFePO_4$ are evaluated using cyclic voltammetry (CV). $LiFePO_4$ samples are used as the working electrode, Ag/AgCl as the reference electrode, and Pt foil as the counter electrode. In CV and GCD techniques, the mass loading is 2 mg cm^{-2}. The specific capacitance (C, F g^{-1}) is first calculated based on the CV curve, using the following formula:

$$C = \int \frac{idV}{2v\Delta Vm}$$

In this context, i, ΔV, m, and v represent current (A), potential window (V), active material mass (g), and scan rate (V s^{-1}), respectively.

$$i = k_1 v + k_2 v^{1/2}$$

The i is the specific current, the *v* is the scanning rate, the $k_1 v$ is the capacity of

pseudocapacitance contribution, and the $k_2 v^{1/2}$ is the diffusive control contribution. The specific capacitance obtained through GCD testing is calculated according to the following formula:

$$C_m = \frac{I \times \Delta t}{m \times \Delta U}$$

where C_m denotes the mass-specific capacitance (F/g), I represents the current (A), Δt denotes the discharge time, m denotes the electrode mass, and ΔU denotes the charge-discharge potential difference.

Supporting figures

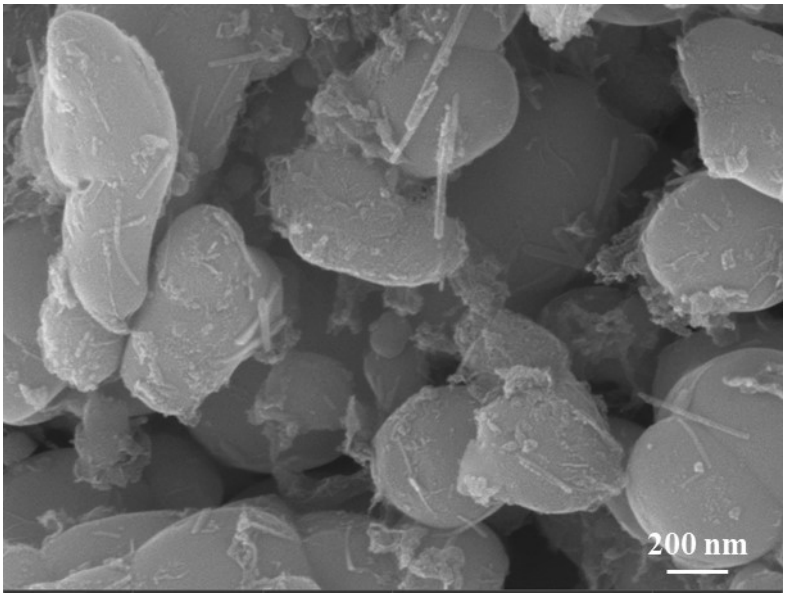

Fig. S1 SEM image of LFP at 200 nm magnification

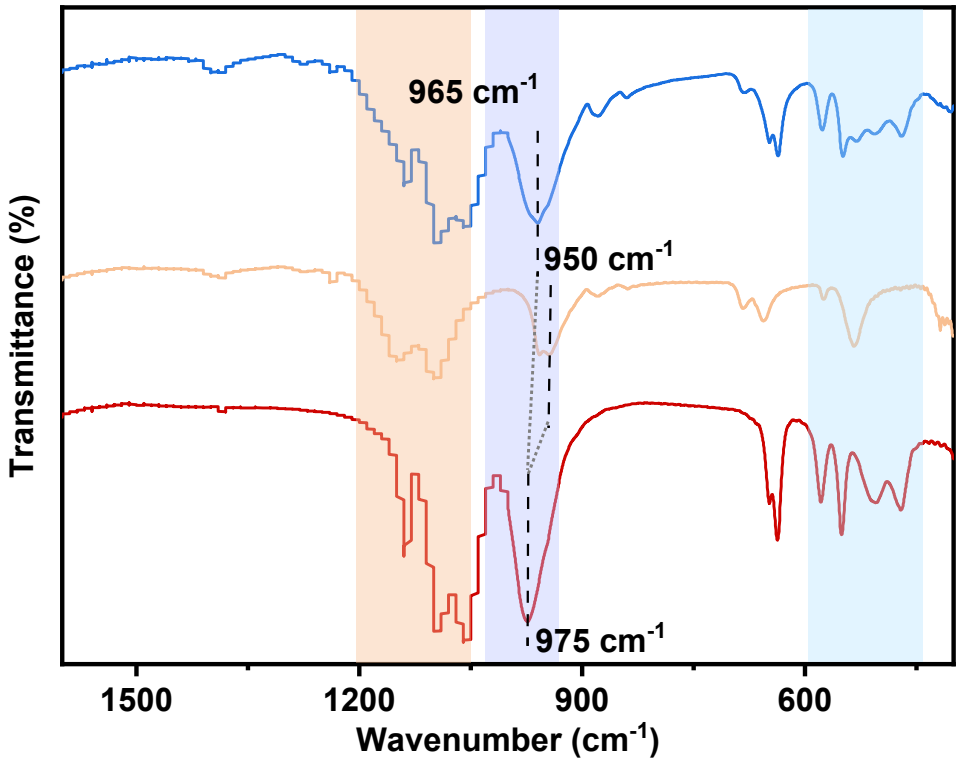

Fig. S2 FT-IR spectra from 300 to 1600 cm^{-1}.

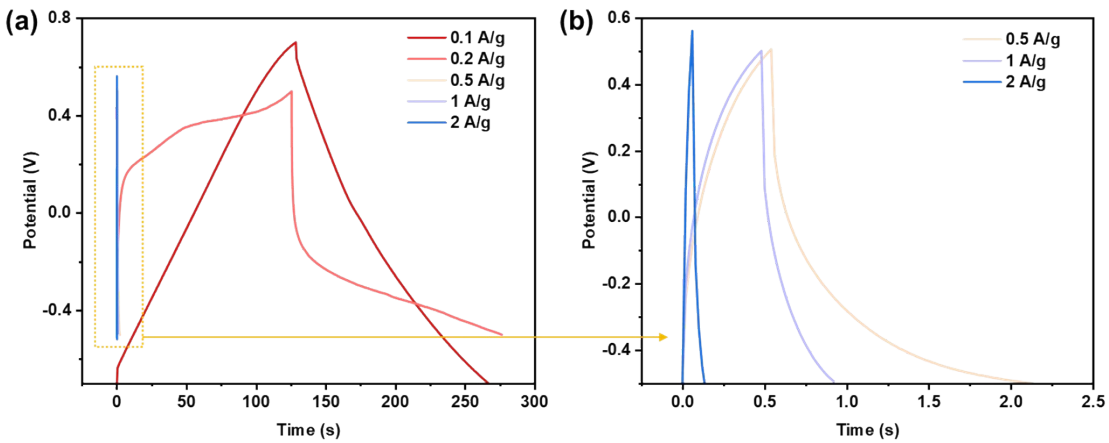

Fig. S3 (a) GCD curves of LFP at different current densities, (b) Magnified view of GCD tests conducted at 0.5, 1, and 2 A/g conditions.

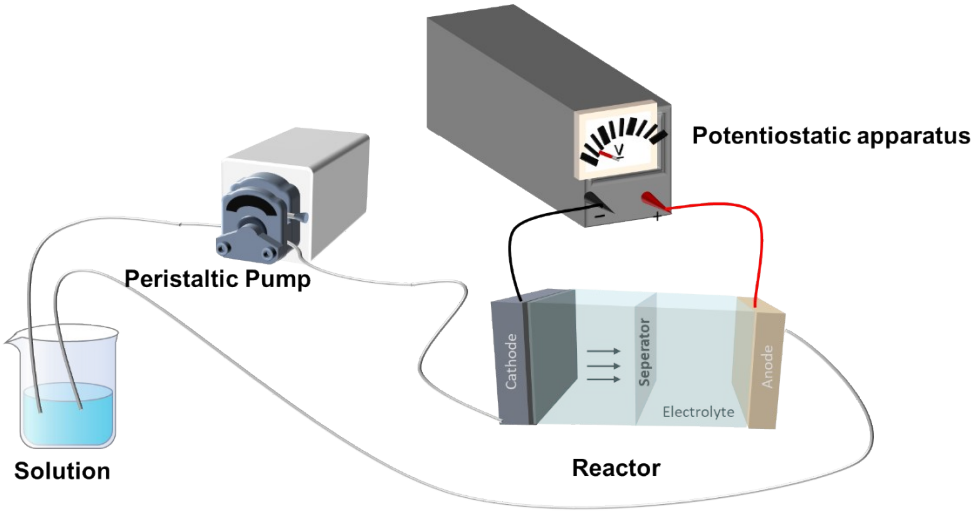

Fig. S4 Schematic Diagram of Capacitive Deionization System.

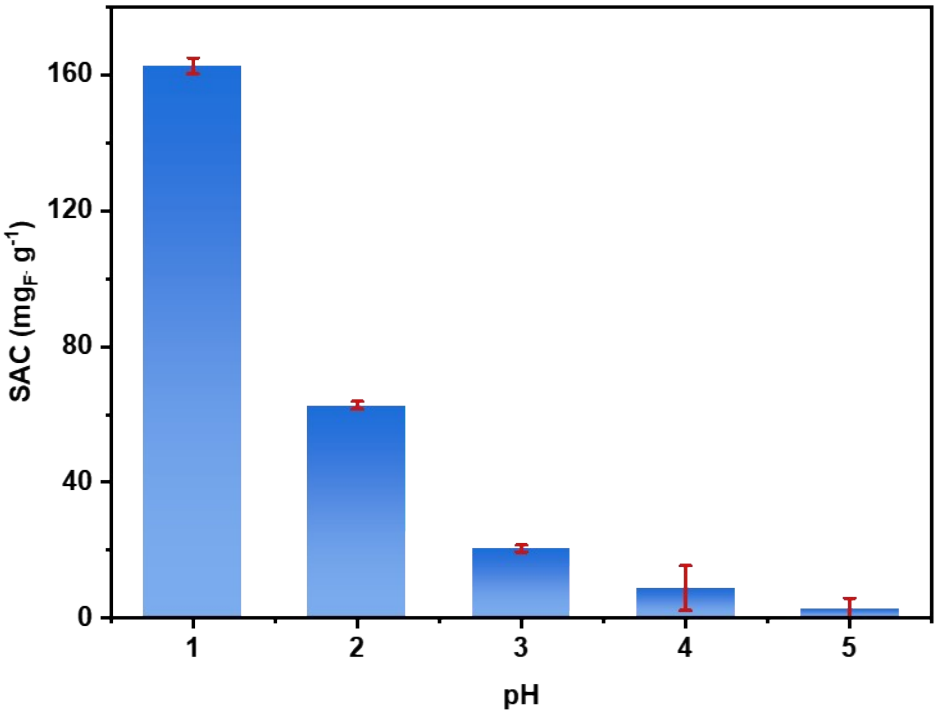

Fig. S5 SAC as a function of pH.

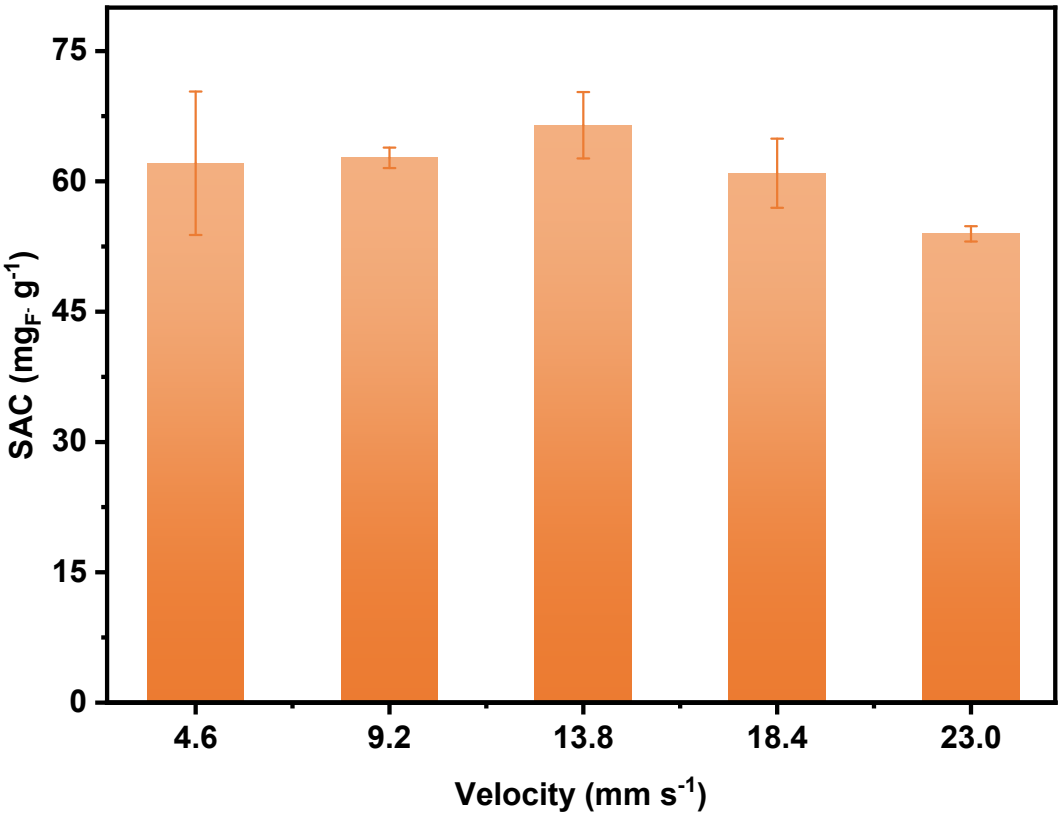

Fig. S6 SAC as a function of flow rate.

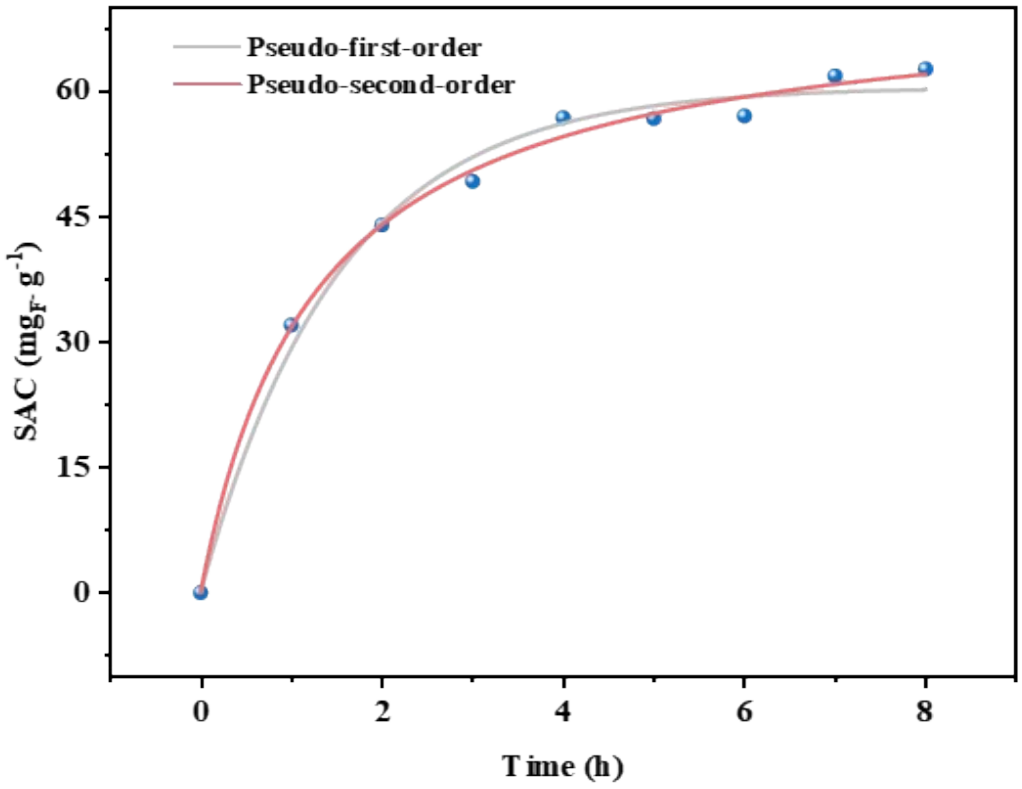

Fig. S7 Kinetic fitting.

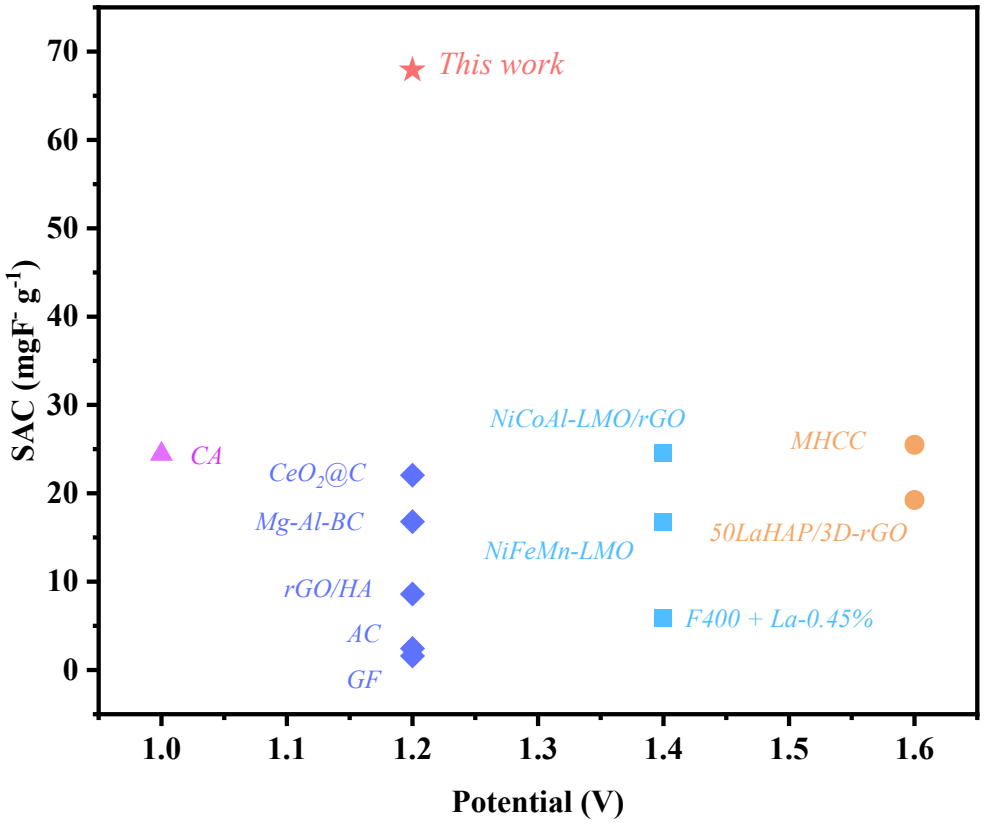

Fig. S8 Comparison of defluorination performance between $LiFePO_4$ and previously reported materials. [1-11]

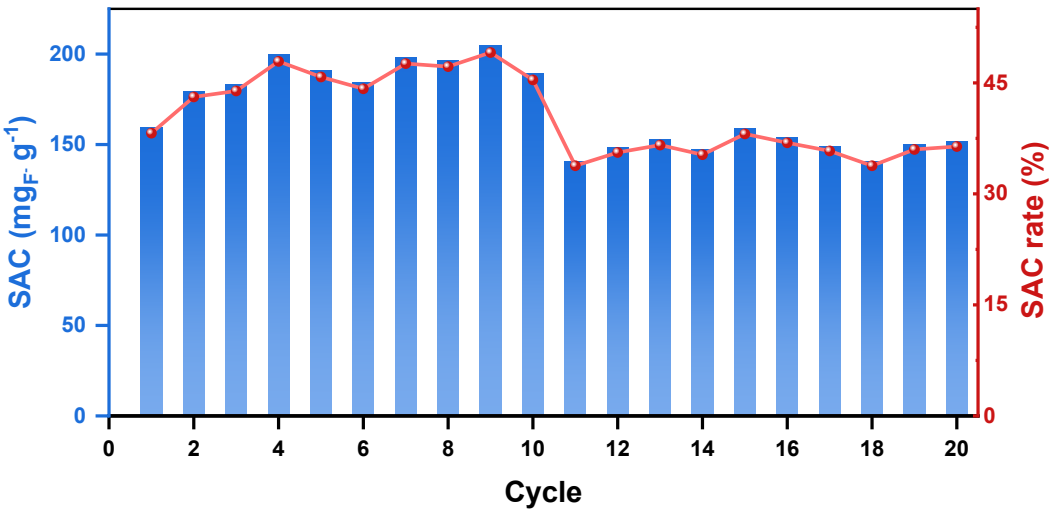

Fig. S9 Desalination performance of LFP after 20 desalination cycles.

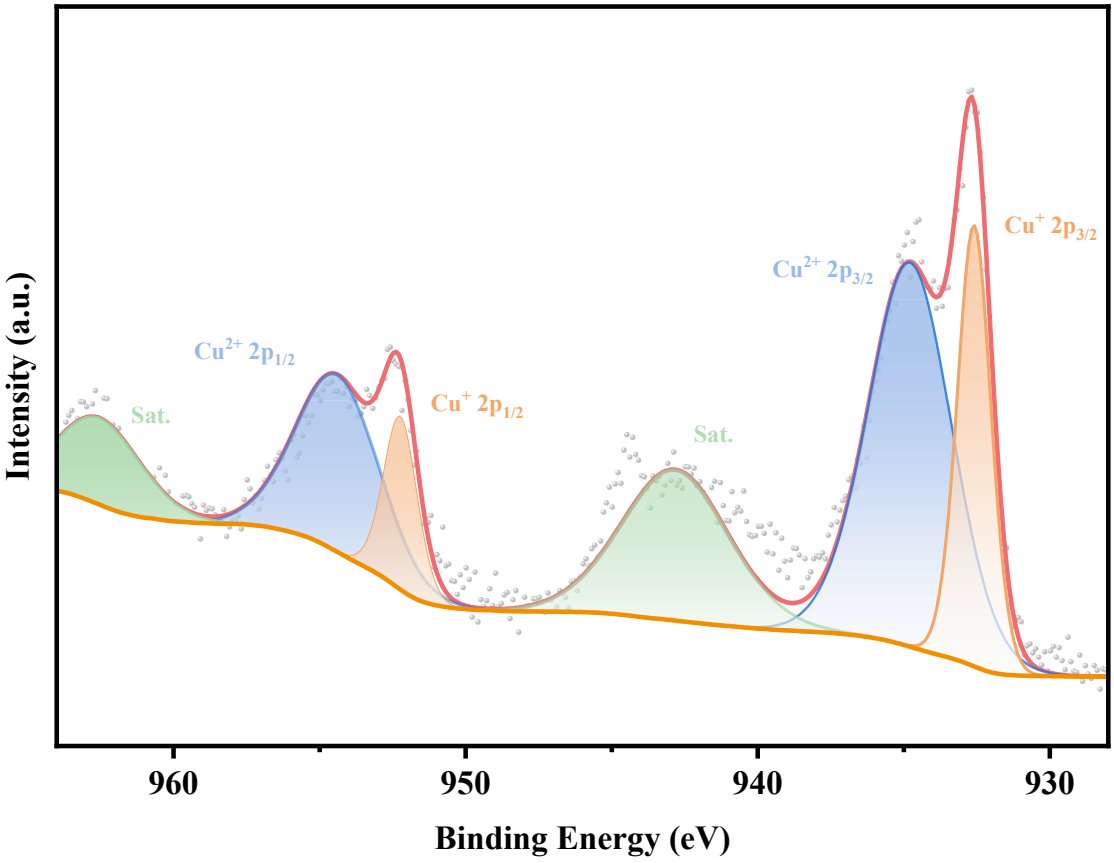

Fig. S10 Fine XPS spectrum of Cu 2p.

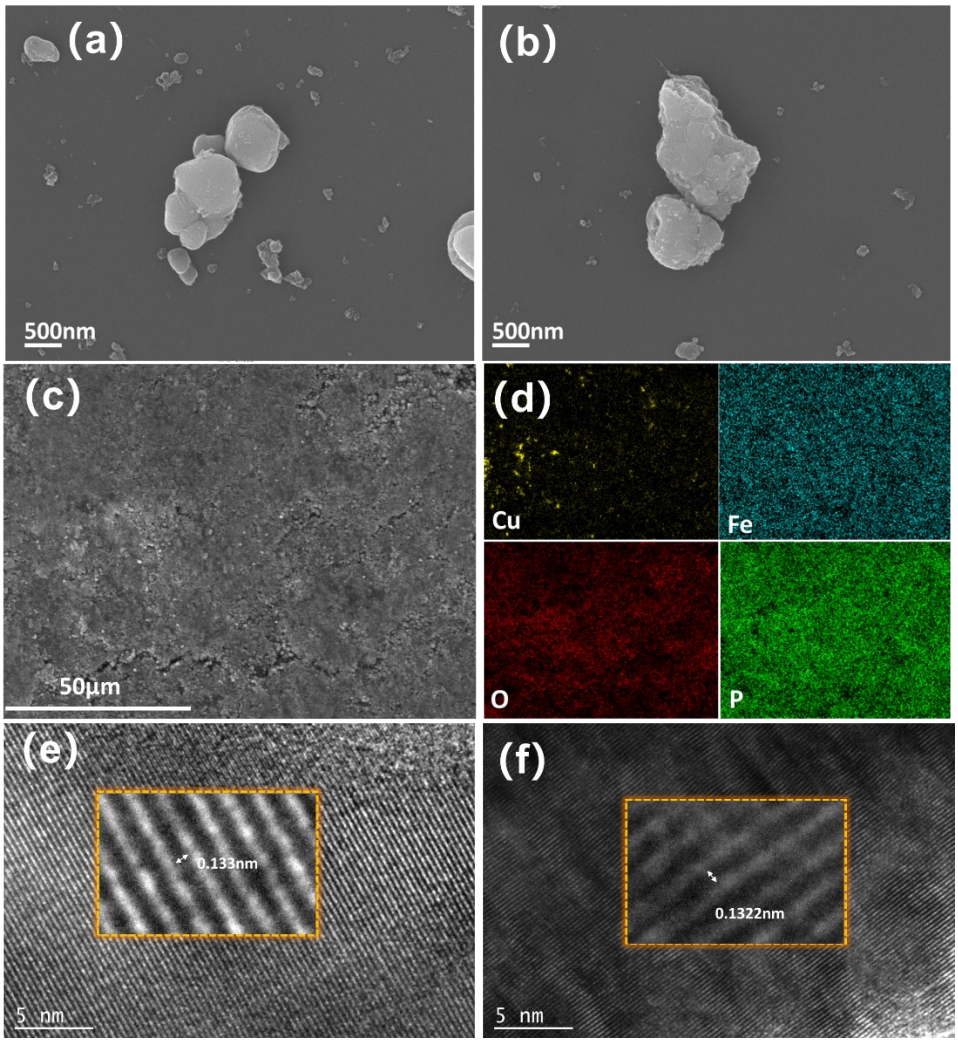

Fig. S11 (a) SEM image of LFP at 500 nm magnification. (b) SEM image of LFP-Cu at 500 nm magnification. (c) SEM image of LFP-Cu at 50 μm magnification. (d) Elemental mapping image of Cu, Fe, O, and P in (c). (e) TEM image of LFP at 5 nm magnification. (f) TEM image of LFP-Cu at 5 nm magnification.

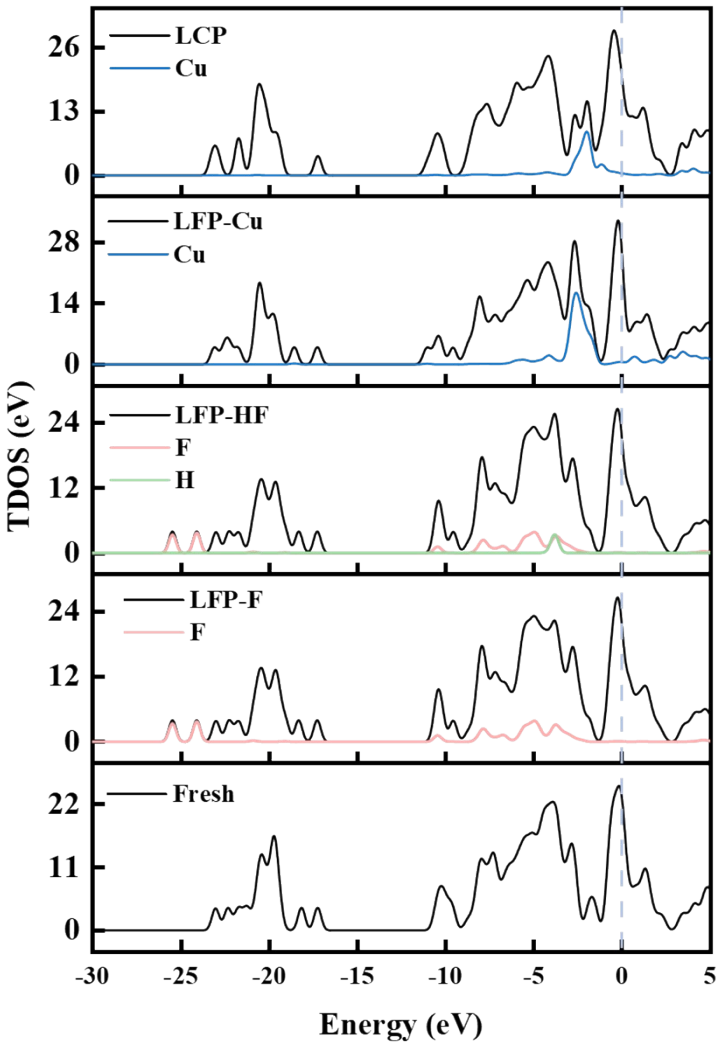

Fig. S12 Total density of states (TDOS) diagram for $LiFePO_4$.

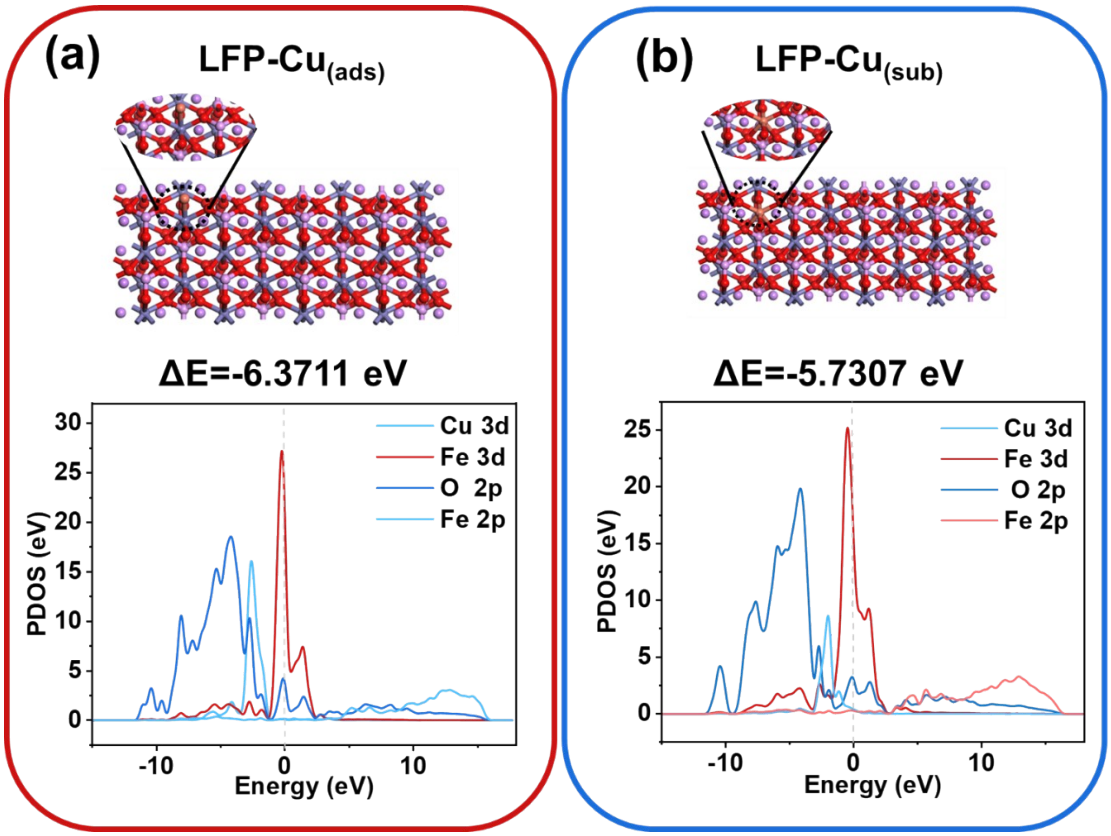

Fig. S13 Adsorption energies and PDOS for different forms of copper ion removal.

Supporting Tables

Table S1 Results of kinetic experiments

Sample	Pseudo-first-order		Pseudo-second-order	
Removal fluoride	q_e (mg/g)	60.43	q_e (mg/g)	71.74
	K_1 (h^{-1})	1.27	K_2 (mg/g/h)	0.0011
	R^2	0.987	R^2	0.995
Removal copper	q_e (mg/g)	203.258	q_e (mg/g)	277.08
	K_1 (h^{-1})	0.159	K_2 (mg/g/h)	0.637
	R^2	0.988	R^2	0.984

Table S2 Comparison of copper removal properties of different materials.

Pollutant	Cathode materials	Potential (V)	Electro-absorption capacity (mg/g)	References
copper	AC	0.8	24.57	[12]
	NPC-0.75	1.2	36.3	[13]
	ACC/ZnO-nPs	1.2	25.14	[14]
	PPy/CS/CNT	0.8	16.8	[15]
	GPCSs	1.2	15.0	[16]
	$LiFePO_4$	1.0	48.62	This work
fluoride	CA	1.0	24.44	[9]
	GF	1.2	1.6	[4]
	AC	1.2	2.44	[2]
	rGO/HA	1.2	8.6	[5]
	Mg-Al-BC	1.2	16.8	[1]
	CeO_2@C	1.2	22.04	[10]
	F400 + La-0.45%	1.4	5.93	[8]
	NiFeMn-LMO	1.4	16.7	[6]
	NiCoAl-LMO/rGO	1.4	24.5	[7]
	50LaHAP/3D-rGO	1.6	19.244	[11]
	MHCC	1.6	25.5	[3]
	$LiFePO_4$	1.2	67.91667	This work

Table S3 Fitted values for the equivalent circuit.

Sample	values	Sample	values
Rs (Ω cm^2)	5.1598	Wo1-R (Ω cm^2)	7.6027×10^{-2}
Rct (Ω cm^2)	1.2745×10^{-3}	Wo1-T (F)	5.2823×10^{-5}
CPE1-T (F)	7.0904×10^{-1}	Wo1--P	3.2102×10^{-1}
CPE1-P	50.324		

Table S4 During the discharge process of GCD testing, the mass-specific capacitance was calculated at different current densities.

current density	Discharge time	Potential	Specific capacitance
0.1	138.5	1.4	9.892857143
0.2	151.06	1	30.212
0.5	1.58	0.185	4.27027027
1	0.2	1.006	0.198807157
2	0.06	0.99672	0.120394895

References

1. G. Wang, D. Chen, Z. Yang, S. Liao, R. S. Tamjidur, S. Hu, Q. Wu and W. Zhang, *Desalination*, 2025, **602**, 118640.
2. X. Zhang, Y. Li, Z. Yang, P. Yang, J. Wang, M. Shi, F. Yu and J. Ma, *Sep. Purif. Technol.*, 2022, **297**, 121510.
3. F. Xiao, Y. Zhou, H. Zhang and Y. Wu, *Sep. Purif. Technol.*, 2024, **328**, 125046.
4. M. S. Gaikwad and C. Balomajumder, *Sep. Purif. Technol.*, 2017, **186**, 272-281.
5. G. Park, S. P. Hong, C. Lee, J. Lee and J. Yoon, *J. Colloid Interface Sci.*, 2021, **581**, 396-402.
6. G. Wang, D. Li, S. Wang, Z. Zhao, S. Lv and J. Qiu, *Sep. Purif. Technol.*, 2021, **254**, 117667.
7. D. Li, S. Wang, G. Wang, C. Li, X. Che, S. Wang, Y. Zhang and J. Qiu, *ACS Appl. Mater. Interfaces*, 2019, **11**, 31200-31209.
8. D. R. Martinez-Vargas, E. R. Larios-Durán, L. F. Chazaro-Ruiz and J. R. Rangel-Mendez, *Sep. Purif. Technol.*, 2021, **268**, 118702.
9. Y. Liu, L. F. Castañeda, O. M. Cornejo and J. L. Nava, *Chemical Engineering and Processing - Process Intensification*, 2023, **190**, 109437.
10. H. Kang, Z. Lu, D. Zhang, H. Zhao, D. Yang, Z. Wang and Y. Li, *Sep. Purif. Technol.*, 2025, **353**, 128551.
11. H. Wang, W. Jiang, P. Nie, B. Hu, Y. Hu, M. Huang and J. Liu, *Electrochim. Acta*, 2022, **429**, 141029.
12. S.-Y. Huang, C.-S. Fan and C.-H. Hou, *J. Hazard. Mater.*, 2014, **278**, 8-15.
13. S. Wang, D. Chen, Z.-X. Zhang, Y. Hu and H. Quan, *Sep. Purif. Technol.*, 2022, **290**, 120912.
14. T. Nguyen Tan and S. Babel, *Journal of Water Process Engineering*, 2023, **56**, 104268.
15. Y.-J. Zhang, J.-Q. Xue, F. Li, J. I. Z. Dai and X.-Z.-Y. Zhang, *Chemical Engineering and Processing - Process Intensification*, 2019, **139**, 121-129.
16. H. Wang, T. Yan, J. Shen, J. Zhang, L. Shi and D. Zhang, *Environmental Science: Nano*, 2020, **7**, 317-326.